

CLINICAL INVESTIGATION

Lung

DOSE-RESPONSE RELATIONSHIP BETWEEN PROBABILITY OF
PATHOLOGIC TUMOR CONTROL AND GLUCOSE METABOLIC RATE
MEASURED WITH FDG PET AFTER PREOPERATIVE
CHEMORADIOTHERAPY IN LOCALLY ADVANCED NON-SMALL-CELL
LUNG CANCER

NOAH C. CHOI, M.D.,* ALAN J. FISCHMAN, M.D., PH.D.,† ANDRZEJ NIEMIERKO, PH.D.,*
JIN-SOOK RYU, M.D.,† THOMAS LYNCH, M.D.,‡ JOHN WAIN, M.D.,§ CAMERON WRIGHT, M.D.,§
PANOS FIDIAS, M.D.,‡ AND DOUGLAS MATHISEN, M.D.§

Departments of *Radiation Oncology, †Radiology, ‡Medicine, and §Surgery, Massachusetts General Hospital, Harvard
Medical School, Boston, MA

Purpose: To determine the dose–response relationship between the probability of tumor control on the basis of pathologic tumor response (pTCP) and the residual metabolic rate of glucose (MRglc) in response to preoperative chemoradiotherapy in locally advanced non–small-cell lung cancer and to define the level of residual MRglc that corresponds to pTCP 50% and pTCP ≥95%.

Methods and Materials: Quantitative dynamic 18F-2-fluoro-2-deoxy-D-glucose (18F-FDG) positron emission tomography was performed to measure regional MRglc at the primary lesion before and 2 weeks after preoperative chemoradiotherapy in an initial group of 13 patients with locally advanced NSCLC. A simplified kinetic method was developed subsequently from the initial dynamic study and used in the subsequent 16 patients. The preoperative radiotherapy programs consisted of (1) a split course of 42 Gy in 28 fractions within a period of 28 days using a twice-daily treatment schedule for Stage IIIA(N2) NSCLC ($n = 18$) and (2) standard once-daily radiation schedule of 45–63 Gy in 25–35 fractions during a 5–7-week period ($n = 11$). The preoperative chemotherapy regimens included two cycles of cisplatin, vinblastine, and 5-fluorouracil ($n = 24$), cisplatin and etoposide ($n = 2$), and cisplatin, Taxol, and 5-fluorouracil ($n = 3$). Patients free of tumor progression after preoperative chemoradiotherapy underwent surgery. The degree of residual MRglc measured 2 weeks after preoperative chemoradiotherapy and 2 weeks before surgery was correlated with the pathologic tumor response. The relationship between MRglc and pTCP was modeled using logistic regression.

Results: Of 32 patients entered into the study, 29 (16 men and 13 women; 30 lesions) were evaluated for the correlation between residual MRglc and pathologic tumor response. Three patients did not participate in the second study because of a steady decline in general condition. The median age was 60 years (range 42–78). One of the 29 patients had two separate lesions, and MRglc was measured in each separately. The tumor histologic types included squamous cell carcinoma ($n = 9$), adenocarcinoma ($n = 13$), large cell carcinoma ($n = 6$), and poorly differentiated carcinoma ($n = 2$). The extent of the primary and nodal disease was as follows: Stage IIB (T3N0M0), Pancoast tumor ($n = 2$); Stage IIIA, T2-T3N2M0 ($n = 18$); Stage IIIB: T1-T3N3M0 ($n = 5$) and T4N0M0 ($n = 2$); a second lesion, T1 ($n = 1$); and localized stump recurrence ($n = 2$). A pathologically complete response was obtained in 14 (47%) of the 30 lesions. The remaining 16 lesions had residual cancer. The mean baseline value of the maximal MRglc was $0.333 \pm 0.087 \mu\text{mol}/\text{min}/\text{g}$ ($n = 16$), and it was reduced to $0.0957 \pm 0.059 \mu\text{mol}/\text{min}/\text{g}$ 2 weeks after chemoradiotherapy ($p = 0.011$). The correlation between residual MRglc and pTCP was made using an increment value of $0.02 \mu\text{mol}/\text{min}/\text{g}$ between the maximal and minimal values of MRglc. A pathologically complete response was obtained in 6 of 6 patients with residual MRglc of $\leq 0.050 \mu\text{mol}/\text{min}/\text{g}$, 3 of 4 with ≤ 0.070 , 4 of 7 with ≤ 0.090 , 0 of 4 with ≤ 0.110 , 1 of 3 with ≤ 0.130 , and 0 of 6 with $\geq 0.130 \mu\text{mol}/\text{min}/\text{g}$. The fitted logistic model showed that residual MRglc corresponding to pTCP 50% and pTCP ≥95% was 0.076 and $\leq 0.040 \mu\text{mol}/\text{min}/\text{g}$, respectively.

Conclusion: The correlation between the gradient of residual MRglc after chemoradiotherapy and pTCP is an inverse dose–response relationship. Residual MRglc of 0.076 and $\leq 0.040 \mu\text{mol}/\text{min}/\text{g}$, representing pTCP 50% and pTCP ≥95%, respectively, may be useful surrogate markers for the tumor response to radiotherapy or chemoradiotherapy in lung cancer. © 2002 Elsevier Science Inc.

Lung cancer, FDG PET, Dose–response relationship.

Reprint requests to: Noah C. Choi, M.D., Department of Radiation Oncology, Massachusetts General Hospital, 100 Blossom St., Boston, MA 02114. Tel: (617) 726-8146; Fax: (617) 726-3603; E-mail: nchoi@partners.org

Presented October 23, 2000 at the 42nd Annual Meeting of the

American Society for Therapeutic Radiology and Oncology, Boston, MA.

Received Mar 21, 2002, and in revised form Jun 24, 2002.

Accepted for publication Jun 24, 2002.

INTRODUCTION

A conventional dose schedule of radiotherapy (RT) administering a total dose of 60 Gy in 30 fractions during a 6-week period is suboptimal in providing tumor control to most patients with Stage III non-small-cell lung cancer (NSCLC) (1–8). Even when combined with a sequential neoadjuvant and consolidation chemotherapy regimen (i.e., a cisplatin-based regimen), the local failure rate remained high at $\geq 70\%$ and the added chemotherapy was able to decrease the distant failure rate from 70% to 49% (5–7).

Dose-response relationships between the radiation dose and local tumor control have been reported in Stage III NSCLC. Perez *et al.* (1) compared four levels of radiation dose: 40 Gy in a split course (20 Gy in five fractions in 1 week, a 2-week rest, and then 20 Gy in five fractions in 1 week) and 40, 50, and 60 Gy administered in 2-Gy dose fractions, five fractions weekly during 4, 5, and 6 weeks in a continuous course of RT for patients with unresectable locoregional NSCLC in a Phase III study. The rate of tumor response was found to be dependent on the radiation dose. The 3-year survival rate was 23%, 10%, and 5% for those with a complete response, partial response, and stable disease, respectively. Choi and Doucette (2) reported a radiation dose-escalation study in which the radiation dose was escalated sequentially from 40–45 Gy to 60–64 Gy using 1.8–2.0-Gy dose fractions, five fractions weekly, for patients with unresectable Stage III NSCLC. Their study showed that the actuarial 3-year survival rate with a minimal follow-up of 2 years was 0%, 5%, 15%, 19%, and 28% for doses of 40–45 Gy ($n = 14$), 46–49 Gy ($n = 40$), 50–55 Gy ($n = 54$), 56–59 Gy ($n = 26$), and 60–64 Gy ($n = 28$), respectively. Saunders *et al.* (8) conducted a Phase III study in which a total dose of 54 Gy administered in 36 fractions during a 12-day period, using 1.5-Gy fractions at three fractions daily, as a continuous hyperfractionated accelerated RT regimen was compared with a conventional dose schedule of 60 Gy in 30 fractions for 6 weeks for patients with medically inoperable Stage I and II and unresectable Stage III NSCLC. The 2- and 3-year survival rate was 30% and 20%, respectively, with the continuous hyperfractionated accelerated RT regimen compared with 21% and 13%, respectively, with the conventional dose schedule ($p = 0.004$). Their study showed that an increase in radiation dose intensity by administering three treatments daily, including the weekend, resulted in an improvement in overall survival. For a subgroup of patients with squamous cell carcinoma, there was a significant decrease in the relative risk of the following: local tumor progression by 21%, metastasis by 24%, and death by 22%.

Therefore, it seems highly likely that an increase in radiation dose and dose intensity in concurrent chemoradiotherapy will lead to an increase in locoregional tumor control beyond that achieved with the current radiation dose schedule of 60 Gy in 30 fractions during 6 weeks and that this gain in locoregional tumor control may be translated into an improvement in survival. A number of Phase I-II

studies have been conducted using either two- or three-dimensional (3D) conformal RT in searching for the maximal tolerated dose of radiation for inoperable and/or unresectable NSCLC (9–14).

Although these Phase I-II studies have been conducted to search for the maximal tolerated dose of radiation and to evaluate its effectiveness in improving locoregional tumor control with concurrent chemoradiotherapy, it is desirable that these studies are also guided by noninvasive biologic imaging studies capable of providing reliable information of the tumor response in a timely manner for individually tailored dose escalation.

Computed tomography (CT) of the chest is the current standard imaging method for restaging lung cancer after RT or chemoradiotherapy. It relies on changes in tumor size in assessing tumor response. Because it may take weeks or even months to know the success or failure of RT or chemoradiotherapy, CT cannot provide useful information in a timely manner for individually tailored escalation of the radiation dose or salvage therapy (15–18).

Warburg (19) described accelerated glucose transport, one of the most characteristic biochemical changes occurring with malignant cellular transformation. A significant increase in the uptake of 2-deoxy-D-glucose and amino acids was reported by Isselbacher (20) when cells were transformed in culture by polyoma virus and simian virus 40. Flier *et al.* (21) evaluated the molecular mechanism of altered glucose transporter activity in cultured rodent fibroblasts transfected with activated myc, ras, and src oncogenes. In cells transfected with myc, the rate of 2-deoxy-D-glucose transport was unchanged. In contrast, transfection with ras and src oncogenes resulted in dramatically increased glucose transport that was paralleled by marked increases in the amounts of glucose transporter protein and messenger RNA. Similarly, exposure of the cells to the tumor-promoting phorbol ester 12-O-tetradecanoyl phorbol 13-acetate also resulted in accelerated glucose transport and increased concentrations of transporter mRNA. Thus, a decrease in glucose metabolism in lung cancer as a result of RT or chemoradiotherapy may be an early marker for subsequent pathologic tumor response.

The glucose analog, 2-fluoro-2-deoxy-D-glucose (FDG) allows measurement of the metabolic rate of glucose (MRglc) representing regional glucose use by quantitative study of 18F-FDG with positron emission tomography (PET) (22–27). Therefore, biologic imaging may be useful in detecting biochemical/metabolic changes in tumor cells as a result of RT or chemoradiotherapy. It is also anticipated that such biochemical changes will occur much sooner than changes in tumor size. Such a change in the metabolic status may be an early biochemical marker for subsequent histopathologic tumor response.

We hypothesize that cessation of glucose uptake by tumor cells after RT or chemoradiotherapy is a reflection of the cell's inability to continue its vital function (i.e., glycolysis). MRglc measured with 18F-FDG uptake after RT or chemoradiotherapy depends on the number and metabolic

activity of the remaining tumor and host cells. No uptake is strong evidence of no residual cells. Residual uptake could reflect the presence of (1) reproductively dead but metabolically intact tumor cells (in full or part) admixed with (2) reproductively intact cells and (3) host cells (28–30). As the dose of fractionated radiation is increased, the number of reproductively intact tumor cells decreases, and the sum of both tumor cell populations also decreases as reproductively dead but metabolically intact cells undergo lysis. The change in the host cell population may not be significant. Therefore, it may be possible to measure MRglc, after radiation or chemoradiotherapy, representing the residual metabolic activities of two groups of the cell population: residual tumor cells that are only metabolically alive but reproductively dead and host cells (tumor stroma) by an *in vivo* assay in a clinical setting. Such a MRglc level is likely to correspond to a subsequent complete tumor response.

The goals of this study were to determine the relationship between the probability of pathologic tumor control (pTCP) and the gradient of residual MRglc in response to RT or chemoradiotherapy in advanced stage NSCLC and to define the level of residual MRglc that corresponds to the $\geq 95\%$ probability of pathologic tumor control (MRglc-pTCP $\geq 95\%$).

METHODS AND MATERIALS

Study plan

The study design consisted of (1) a measurement of the rate constants, K_1 , k_2 , and k_3 , of a three-compartment metabolic model using quantitative dynamic 18F-FDG PET before and 2 weeks after preoperative RT or chemoradiotherapy in patients with locally advanced NSCLC; (2) calculation of MRglc using the measured value of K_1 , k_2 , k_3 , and the formula $\text{MRglc} = \text{Pglc}/\text{LC} \times [K_1 \times k_3/(k_2 + k_3)]$ $\mu\text{mol}/\text{min}/\text{g}$, where LC is the lumped constant, assumed to be 1 and corrected for plasma glucose (Pglc); and (3) correlation of residual MRglc after preoperative RT or chemoradiotherapy with the pathologic tumor response in patients with Stage III NSCLC. The rate constants K_1 and k_2 are the rates of 18F-FDG transport from plasma into tissue and from tissue back into plasma, and k_3 is the rate of 18F-FDG phosphorylation. The rate of 18F-FDG dephosphorylation was assumed to be 0. The LC is represented by the formula $\text{LC} = \text{MRfdg}/\text{MRglc}$ (where MRfdg is the metabolic rate of FDG) and indicates the different affinities of FDG and glucose for transportation and phosphorylation.

Patients

Patients with Stage IIIA (N2) NSCLC who were enrolled into an institutional Phase II study for preoperative chemoradiotherapy were accrued to this study. This was conducted as a companion study with informed consent approved by the Subcommittee on Human Studies. Also eligible for this study were patients with potentially operable Pancoast tumor (T3-T4N0M0 lesion), a highly selected subset of patients with Stage IIIB (T1-T3N3M0, T4N0M0) NSCLC,

and patients with recurrent tumor limited to the bronchial stump after prior lobectomy judged potentially resectable after preoperative chemoradiotherapy.

Preoperative therapy

The treatment program of the institutional Phase II study consisted of preoperative concurrent chemoradiotherapy, surgery on Day 57, and postoperative chemoradiotherapy. The details of the program and results of this Phase II study were reported earlier (31). In brief, the preoperative RT consisted of split-course RT in which a total dose of 42 Gy was administered in two sessions using a twice-daily treatment schedule: (1) 21 Gy in 1.5-Gy fractions, twice daily, with an intertreatment interval of 5 h, 5 days weekly for 7 treatment days starting on Day 1 with the first course of chemotherapy; (2) a 10-day rest; and (3) an additional dose of 21 Gy in the same way as the first starting on Day 19. Postoperatively, patients received two levels of additional doses: Either 18 Gy for positive resection margins or gross residual tumor in the resected specimen or 12 Gy for microscopic residual disease only or a pathologically complete response using the same twice-daily treatment schedule for a total dose of 60 Gy and 54 Gy, respectively. Postoperative RT was started on Day 85 with the third course of concurrent chemotherapy. Patients with Stage IIIA, N2 disease were treated with this program ($n = 15$).

The chemotherapy regimen consisted of three courses, two courses preoperatively beginning on Days 1 and 29 and the third starting on Day 85, 1 month after surgery. The chemotherapy regimen for patients with Stage IIIA, N2 NSCLC ($n = 15$) consisted of 5-fluorouracil 30 mg/kg/d by 72-h continuous i.v. infusion beginning Day 1 of each cycle, cisplatin 100 mg/m² i.v. for 30 min with prior hydration, 2–6 h after initiating 5-fluorouracil on Day 1, and an i.v. bolus of vinblastine 4 mg/m² on Day 1 of each cycle. Patients with Stage IIIB NSCLC ($n = 7$) and stump recurrence ($n = 2$) were administered the same chemotherapy regimen as above with concurrent RT of 54–63 Gy in 30–35 fractions during a 6–7-week period. For patients with Pancoast tumor, T3N0M0 lesion ($n = 2$), preoperative therapy consisted of cisplatin 50 mg/m² on Days 1, 8, 29, 36; etoposide 50 mg/m² on Days 1–5 and 29–33; and concurrent RT of 45 Gy in 25 fractions during a 5-week period. Patients who were entered into a new preoperative chemoradiotherapy protocol in 1998 and 1999 were treated with a chemotherapy regimen of cisplatin 33 mg/m²/d i.v. for 1–2 h on Days 2–4 (cycle 1) and Days 30–32 (cycle 2), 5-fluorouracil 800 mg/m²/d by 24-h continuous infusion on Days 1–4 and 29–32, and paclitaxel 100 mg/m² i.v. by 3-h infusion on Days 1 and 29, and preoperative concurrent radiation of 45 Gy in 25 fractions within a 5-week period ($n = 3$). Growth factors were not given as a part of this protocol.

After preoperative chemoradiotherapy, all patients underwent restaging with CT of the chest and upper abdomen, bone scan, and CT of the head. Patients who remained free of distant metastasis underwent thoracotomy 4 weeks after

completion of preoperative therapy with the aim of complete resection of the primary lesion and involved regional lymph nodes.

Quantitative dynamic 18F-FDG PET

18F-FDG PET imaging was performed with an eight-ring whole-body imaging system (Scanditronix PC4096-16WB, Uppsala, Sweden). The primary imaging parameters of this instrument are an in-plane and axial resolution of 7.0-mm full width (of photopeak measured at) half maximal (count) (FWHM), 15 contiguous slices of 6.5-mm separation and sensitivity of 5000 cps/ $\mu\text{Ci}/\text{cm}^3$. All images were reconstructed using a conventional filtered back-projection algorithm to an in-plane resolution of 7-mm FWHM. Transmission scans acquired with a rotating pin source containing ^{68}Ge were used to confirm the positioning and to correct for tissue attenuation. All projection data were corrected for nonuniformity of detector response, dead time, random coincidences, and scattered radiation. The PET camera was cross-calibrated against a well scintillation counter by comparing the camera response from a uniform distribution of an 18F solution in 20-cm cylindrical phantom with the response of well counter to an aliquot of the same solution.

The Human Studies Committee of the Massachusetts General Hospital approved the 18F-FDG PET study protocol, and each patient provided written informed consent. Paired studies were to be obtained in each patient whenever it was feasible. The first and second studies were performed a few days before treatment began and 2 weeks after the preoperative therapy completion, respectively. The patients fasted for at least 6 h before imaging. Immediately before the study, the blood glucose concentration was determined. The detailed procedure of this quantitative dynamic 18F-FDG PET study has been reported earlier (25). In brief, patients were positioned supine on the imaging bed of the PET camera with arms extended out of the field of view. Dynamic image collection was started immediately before i.v. injection of 10 mCi of 18F-FDG. Sequential images were acquired in 15-s frames for the first 1.75 min, 30-s frames for the next 2 min, 60-s frames for the next 2 min, 2-min frames for the next 4 min, 5-min frames for the next 20 min, 10-min frames for the next 40 min, and a final 15-min frame for the final 15 min. At the conclusion of imaging, the emission and transmission images were reconstructed using a conventional filtered back-projection algorithm to an in-plane resolution of 7-mm FWHM.

Arterial input curves were measured from both arterial blood samples and left ventricular time activity curves in 6 patients and from the left ventricular time activity curves alone in 7 patients (32). The use of left ventricular time-activity curves as arterial input functions is a well-established technique. In addition, in the 6 patients studied, the analysis was performed both with left ventricular time-activity curves and curves obtained by direct sampling. In all cases, the results were essentially identical.

Areas of the tumor were screened for analysis using a constant circular region of interest (ROI) with a 16-mm

diameter. The regions were positioned over areas of tumor with high metabolic activity, thus avoiding any apparent necrotic areas. Of the several possible methods for defining ROIs, we believed that a fixed ROI centered over the region of greatest FDG activity on the 90-min scan was the most appropriate. This type of ROI is very convenient for comparisons between repeated studies. This dynamic method was used for the initial 13 patients.

Simplified kinetic method of 18F-FDG PET

After the initial 13 patients completed the quantitative dynamic 18F-FDG PET study for the measurement of MRglc, we developed a simplified kinetic method based on the measured blood curves from a control group that requires a correction for blood glucose concentration in the beginning of the study and one venous blood sample at the end of the imaging for blood 18F-FDG activity. It was found out that the coefficient of determination between MRglc measured with the dynamic and simplified methods was 0.96, 0.94, and 0.98 for pretherapy, posttherapy, and pooled data. Thus, the observed tumor tissue uptake of 18F-FDG, corrected for blood 18F-FDG activity and glucose concentration, can reliably predict the MRglc from a single static image acquired at between 45 min and 1 h after injection. The details of the dynamic study and the simplified kinetic method have been reported earlier (26).

This simplified kinetic method was used for the remainder of the study. For this method, approximately 10 mCi (370 MBq) of 18F-FDG was injected intravenously as a bolus after the patient had fasted for ≥ 6 h. The blood glucose levels were measured just before injection of 18F-FDG. The static emission images began about 45 min after injection of 18F-FDG. The patients underwent imaging in three contiguous bed positions over the chest; each scan was 10 min. A blood sample was obtained at the end of the imaging for the correction of blood 18F-FDG activity.

Several areas of the tumor were screened for analysis by selecting the ROI over the highest 18F-FDG activity in the tumor as visualized in the final acquisition. From the images acquired between 45 and 60 min, the value of MRglc for tumor tissue was calculated according to the simplified kinetic method by correcting the observed 18F-FDG activity at 55 min with the blood 18F-FDG activity at 55 min and the blood glucose concentration. The MRglc of the primary tumor was determined using the maximal value in the ROI positioned over the area with the highest activity as determined by visual analysis. When little or no tumor-related radioactivity was discernible by visual analysis (posttherapy studies), the ROI was positioned on the basis of CT scan data.

Statistical analysis

The relationship between MRglc and pTCP was modeled using logistic regression. As a secondary analysis, logistic regression analysis was used to test the significance of MRglc for pathologic tumor control (33–35). To determine the sensitivity and specificity of the relationship between

Table 1. Patient characteristics

Patients (<i>n</i>)	29
Lesions (<i>n</i>)	30
Median age (y)	60 (42–78)
Gender (<i>n</i>)	
Male	16
Female	13
Histologic type (<i>n</i>)	
Squamous cell carcinoma	9
Adenocarcinoma	13
Large cell carcinoma	6
Poorly differentiated carcinoma	2
Tumor stage	
IIB	
T3N0M0	2
IIIA	
T2N2M0	13
T3N2M0	5
IIIB	
T1-T3N3M0	5
T4N0M0	2
Second lesion, T1	1
Stump recurrence	2

MRglc and pTCP, receiver operating characteristic analysis and Hosmer-Lemshow goodness-of-fit tests were performed (36, 37).

RESULTS

Patient characteristics

The study began in April 1992 with a limited availability of 18F-FDG PET for study patients with lung cancer. Of 32 patients who were entered into the study, 29 (16 men and 13 women; 30 lesions) were available for assessment for the correlation between residual MRglc and pathologic tumor response. Three patients did not undergo the second study because of a steady decline in general condition. Thirteen of the 29 patients were enrolled between 1992 and 1994. The next 16 patients were enrolled between 1997 and 1999. The demographics of these patients and the tumor stage are presented in Table 1. The median age was 60 years (range 42–78). One of the 29 patients had two separate lesions for which MRglc was measured in each separately. The tumor histologic types included squamous cell carcinoma (*n* = 9), adenocarcinoma (*n* = 13), large cell carcinoma (*n* = 6), and poorly differentiated carcinoma (*n* = 2). The extent of the primary and nodal disease was as follows: Stage IIB (Pan-coast tumor), T3N0M0 (*n* = 2); Stage IIIA, T2-T3N2M0 (*n* = 18); Stage IIIB: T1-T3N3M0 (*n* = 5) and T4N0M0 (*n* = 2); a second lesion, T1 (*n* = 1); and localized stump recurrence (*n* = 2).

Tumor response

The tumor response was measured 1 month after completion of the preoperative therapy. A complete pathologic response of both the primary lesion and the involved lymph nodes was obtained in 11 (38%) of 29 patients. For the primary lesion (*n* = 27), localized stump recurrence (*n* =

2), and the second primary lesion (*n* = 1), a complete pathologic response was obtained in 14 (47%) of the 30 lesions. The remaining 16 lesions showed residual cancer. Among those with N2 lesions, conversion from N2 to N0 was noted in 11 (58%) of 19 patients.

MRglc measured using a three-compartment model

The metabolic rate of 18F-FDG representing MRglc was calculated using a three-compartment model. The details of the measurement of the rate constants, K1, k2, and k3, and the calculation of the deoxyglucose metabolic rate were reported earlier (26). The mean values for the rate constants K1, k2, and k3 of the initial 13 patients derived from the three-compartment model were as follows: K1 remained essentially unchanged at $0.0781 \pm 0.0243 \text{ min}^{-1}$ before treatment to $0.0774 \pm 0.030 \text{ min}^{-1}$ after treatment; k2 increased from $0.0271 \pm 0.023 \text{ min}^{-1}$ before treatment to $0.0835 \pm 0.0189 \text{ min}^{-1}$ after treatment ($p < 0.01$); and k3 was markedly decreased from $0.0592 \pm 0.0178 \text{ min}^{-1}$ before treatment to $0.0176 \pm 0.0030 \text{ min}^{-1}$ after treatment ($p < 0.01$). The metabolic rate of deoxyglucose was calculated using the measured value of K1, k2, and k3 from the dynamic uptake study and the formula $\text{MRglc} = \text{Pglc}/\text{LC} \times [\text{K1} \times \text{k3}/(\text{k2} + \text{k3})] \mu\text{mol}/\text{min}/\text{g}$ for the initial 13 patients. The LC was assumed to be 1.0 in lung cancer.

For the remaining 16 patients with 17 lesions, it was measured using a simplified kinetic method also described in detail in an earlier report (26). Because of the limited availability of the FGD-PET studies with short notice and a long waiting period, FDG-PET was obtained in only 16 of 29 patients (17 of 30 lesions) before preoperative therapy was started. In these 16 patients, the mean MRglc before preoperative therapy was $0.333 \pm 0.087 \mu\text{mol}/\text{min}/\text{g}$ and was reduced to $0.0957 \pm 0.059 \mu\text{mol}/\text{min}/\text{g}$ 2 weeks after completion of preoperative therapy. This represents a 71% decrease ($p = 0.011$) from the pretherapy value.

Residual MRglc after chemoradiotherapy or RT and its correlation with pathologic tumor control

The rate of pathologic tumor control was correlated with the residual MRglc using an increment value of $0.02 \mu\text{mol}/\text{min}/\text{g}$ between the maximal and minimal values of MRglc. An inverse dose-response relation was noted between the magnitude of residual MRglc and the rate of complete pathologic tumor response (Table 2). A complete pathologic response was noted in 6 of 6 patients when the residual MRglc was $\leq 0.050 \mu\text{mol}/\text{min}/\text{g}$. In contrast, no complete pathologic response was observed in any of 6 patients when the residual MRglc was $\geq 0.130 \mu\text{mol}/\text{min}/\text{g}$.

Analysis and modeling of tumor response as a function of deoxyglucose metabolic rate

The following logistic model of pTCP as a function of the logarithm of MRglc was investigated (33–35):

$$\ln\left(\frac{\text{pTCP}}{1-\text{pTCP}}\right) = \beta_0 + \beta_1 \ln(\text{MRglc})$$

Table 2. Residual MRglc after radiotherapy or chemoradiotherapy and corresponding pathologic tumor control

Residual MRglc ($\mu\text{mol}/\text{min}/\text{g}$)	Tumor control (%)
≤ 0.050 (0.009–0.048)	6/6 (100)
≤ 0.070 (0.054–0.064)	3/4 (75)
≤ 0.090 (0.071–0.082)	4/7 (57)
≤ 0.110 (0.096–0.107)	0/4 (0)
≤ 0.130 (0.115–0.127)	1/3 (33)
≥ 0.130 (0.131–0.211)	0/6 (0)

Abbreviation: MRglc = metabolic rate of glucose.

Numbers in parentheses are the range, unless otherwise noted.

The logarithm of MRglc was used (instead of MRglc itself), because MRglc can have only positive values and because the distribution of MRglc levels in the population of patients is likely to be positively skewed.

The maximal likelihood estimates of the model parameters were obtained and were as follows: $\beta_0 = -12.0$ (95% confidence interval [CI] -21.1 to -3.0) and $\beta_1 = -4.7$ (95% CI -8.2 to -1.1).

The value of MRglc₅₀ (level of MRglc corresponding to a 50% chance of tumor control) and the corresponding 95% CI were estimated using Fieller's theorem (35). In addition, the values of MRglc₉₀ (level of MRglc corresponding to a 90% chance of tumor control) and MRglc₉₅ (level of MRglc corresponding to a 95% chance of tumor control) were also estimated. These values were as follows: MRglc₅₀ = 0.076 (95% CI 0.051–0.11); MRglc₉₀ = 0.047 (95% CI 0.009–0.064); MRglc₉₅ = 0.040 (95% CI 0.005–0.057).

The goodness-of-fit model was evaluated using the Pearson chi-square test and Hosmer-Lemeshow test: Pearson chi-square = 22.5 (26 degrees of freedom), p greater than chi-square = 0.66; Hosmer-Lemeshow chi-square = 0.71 (data divided into five groups on the basis of the predicted probability), p greater than chi-square = 0.87. According to both tests, the model fit the data well.

A comparison of the observed pathologic tumor response and model predictions is shown in Table 3. The pathologic response was 1 if the tumor was controlled. The level of MRglc, the observed pathologic response, and the corresponding predicted probability of pathologic tumor control for all 30 lesions are shown. The classification statistics are shown in Table 4 in which T0 represents pathologic tumor control and greater than T0 represents no tumor control; the classification was positive if the predicted probability (TCP) was >0.5 . On the basis of the values in Tables 3 and 4 and assuming a cutoff of 0.5, we calculated the sensitivity of the model as 86%, the specificity as 81%, the positive predictive value as 80%, and the negative predictive value as 87%. The percentage of cases correctly classified was 83% (i.e., 25 of 30 cases).

The receiver operating characteristic curve showing sensitivity vs. one minus specificity is presented in Fig. 1. The area under the curve, which was 0.90, suggested a good predictive power of the model (a model with no predictive power has an area of 0.5; a perfect model has an area of 1).

Table 3. Comparison of observed pathologic tumor response and model predictions

Pt. No.	MRglc ($\mu\text{mol}/\text{min}/\text{g}$)	Pathologic response	Model prediction
1	0.009	1	~1
2	0.017	1	~1
3	0.019	1	~1
4	0.032	1	0.98
5	0.042	1	0.94
6	0.048	1	0.90
7	0.054	1	0.84
8	0.056	1	0.81
9	0.058	0	0.79
10	0.064	1	0.70
11	0.071	1	0.59
12	0.071	0	0.59
13	0.074	0	0.54
14	0.075	1	0.52
15	0.076	1	0.51
16	0.077	0	0.49
17	0.082	1	0.42
18	0.096	0	0.26
19	0.096	0	0.26
20	0.107	0	0.17
21	0.108	0	0.17
22	0.115	0	0.13
23	0.117	0	0.12
24	0.127	1	0.08
25	0.131	0	0.07
26	0.143	0	0.05
27	0.159	0	0.03
28	0.171	0	0.02
29	0.200	0	0.01
30	0.211	0	<0.01

Abbreviations: Pt. No. = patient number; MRglc = metabolic rate of glucose.

Figure 2 shows the sensitivity and specificity of the model vs. the probability cutoff. For a probability cutoff of 0.5, the corresponding sensitivity and specificity was 86% and 81%, respectively. Both values suggest that the model has good predictive value.

Figure 3 shows the fitted logistic model of pTCP as a function of residual MRglc with the corresponding 95% CI. The residual MRglc corresponding to a pTCP of 50% and pTCP of $\geq 95\%$ was 0.076 $\mu\text{mol}/\text{min}/\text{g}$ and ≤ 0.040 $\mu\text{mol}/\text{min}/\text{g}$, respectively.

Table 4. Classification statistics

Classified	True (n)		Total (n)
	T0	$>T0$	
+	12	3	15
–	2	13	15
Total (n)	14	16	30

Abbreviations: T0 = pathologic tumor control; $>T0$ = no tumor control.

Classified + if predicted probability >0.5 .

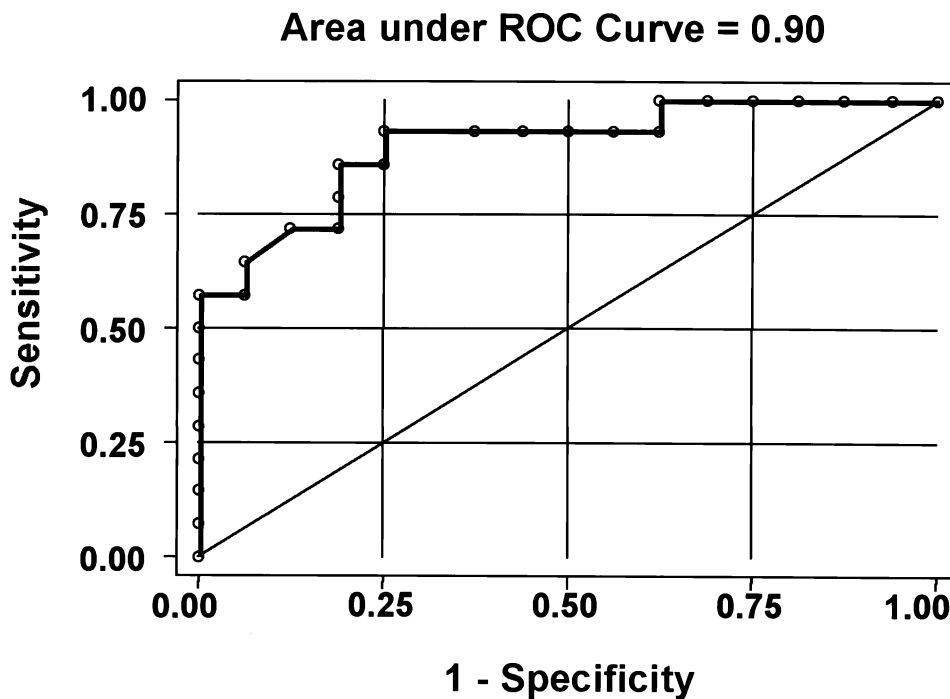


Fig. 1. Receiver operating characteristic (ROC) curve showing sensitivity vs. one minus specificity. The area under the curve was 0.90, suggesting good predictive power of the model (a model with no predictive power has an area of 0.5 and a perfect model has an area of 1).

DISCUSSION

FDG PET studies, in establishing a diagnosis of lung cancer and assessing tumor response to RT or chemoradio-

therapy, have been interpreted using the following methods: (1) qualitative (visual reading method); (2) semiquantitative (i.e., differential uptake ratio [DUR] or standard uptake value [SUV] representing the difference in FDG uptake

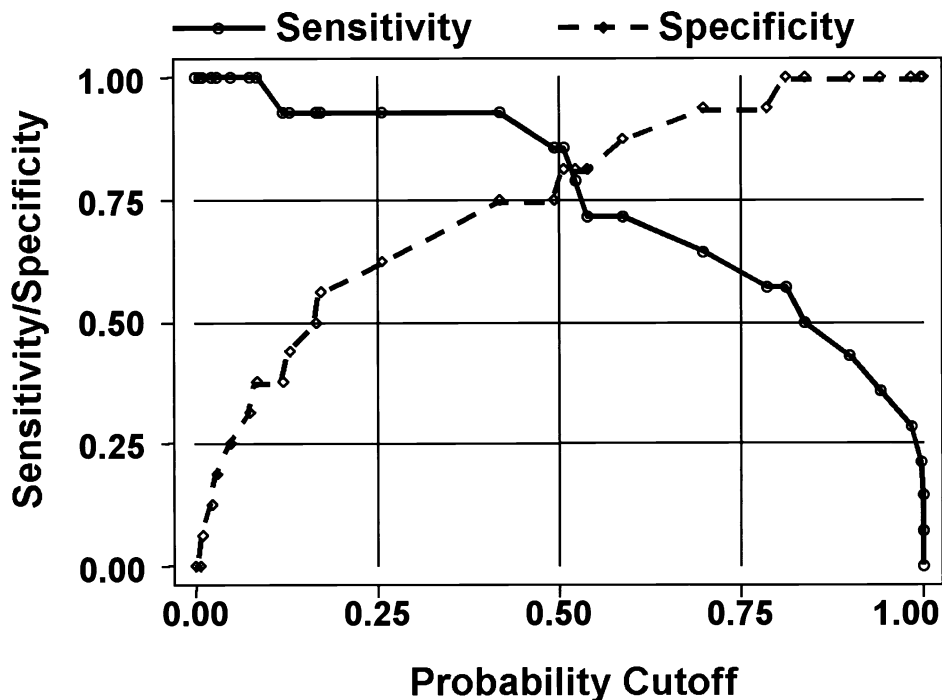


Fig. 2. Sensitivity and specificity of the model vs. probability cutoff. For a probability cutoff of 0.5, the corresponding sensitivity was 86% and specificity was 81%. Both values suggest that the model has a good predictive value.

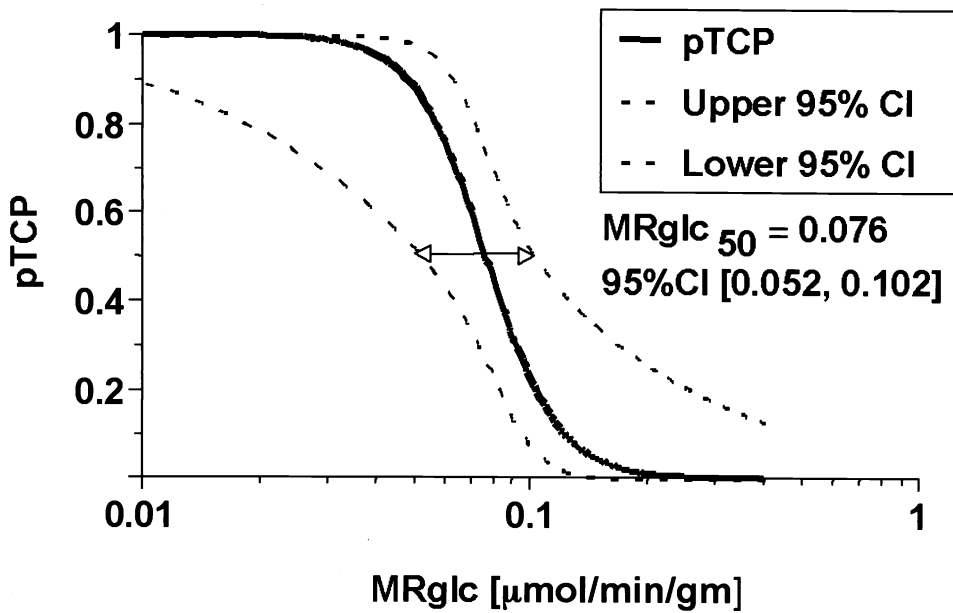


Fig. 3. Fitted logistic model of pTCP based on pathologic tumor control as a function of MRglc with corresponding 95% CIs. The abscissa is in log scale.

between the ROI placed over the tumor and the background activity in the normal tissue normalized to body weight); and (3) quantitative using three-compartment modeling (38).

Visual interpretation and the DUR-based method of 18F-FDG PET image analysis have been used to diagnose primary lung cancer clinically and detect metastatic disease at either the regional lymph nodes or distant organs (39–47). In a meta-analytic comparison of FDG PET and CT in detecting mediastinal nodal metastasis in NSCLC (29 studies, 2226 patients), Dwamena *et al.* (43) reported that the sensitivity and specificity was 79% and 91%, respectively, for FDG PET and 60% and 77%, respectively, for CT. FDG PET has also been reported to be effective in detecting recurrent disease after surgery, RT, or chemoradiotherapy (48, 49).

The qualitative interpretation for tumor response after RT or chemoradiotherapy is helpful when no residual FDG uptake is present in the tumor or a new lesion appears. However, the interpretation becomes difficult and subjective when the changes in FDG uptake are subtle. In current practice, the SUV of FDG PET is obtained at 45–60 min after administration of 18F-FDG. However, the optimal timing for measuring FDG uptake remains controversial. It has been shown that FDG uptake in lung cancer may not reach the maximal plateau value within 60 min after administration of 18F-FDG (50–53). In fact, Hamberg *et al.* (25) showed that it takes 2–3 h to reach the plateau value of uptake after administration of 18F-FDG in Stage III NSCLC. Lowe *et al.* (54) performed a dynamic FDG PET study to determine the optimal time for emission data acquisition in 14 patients with focal pulmonary abnormalities, 10 with malignant and 4 with benign lesions by biopsy.

Dynamic PET data were acquired as sequential 5-min images for 2.5 h. However, the DUR values provided the greatest separation between benign and malignant abnormalities beginning at 50 min and no advantage was realized by later imaging. The tumor size may make a difference in the period between the injection of 18F-FDG and the time to reach the maximal uptake value. Patients with focal pulmonary abnormalities were studied by Lowe *et al.*, but patients in the study by Hamberg *et al.* had Stage III NSCLC. It is well described that regions with a poor blood supply and hypoxia are more frequent with larger tumors than with small ones. Therefore, the FDG uptake at 45–60 min after administration of 18F-FDG may be an underestimation of the true value of FDG uptake in large tumors or tumors with hypoxic regions. Pitfalls in the interpretation of FDG PET using visual reading and DUR in lung cancer have been described (55–58).

Regional glucose metabolism was originally measured using an autoradiographic method and three-compartment model by Sokoloff *et al.* (22) in brain tissue. Phelps *et al.* (23) used FDG PET to measure regional MRglc in the human brain and validated the method. Patlak *et al.* (24) introduced a graphic analysis method in measuring regional MRglc in brain in which dephosphorylation (k₄) is assumed to be negligible.

We explored a quantitative kinetic method of 18F-FDG uptake in Stage III NSCLC to determine the characteristics of the FDG uptake curve and measure the maximal value at the plateau phase of uptake. We measured the rate constants, K₁, k₂, and k₃, of the three-compartment model to calculate the MRglc. Because the dynamic method requires continuous imaging for 80 min after the administration of 18F-FDG, it is a very difficult procedure to undergo for

most patients with advanced-stage lung cancer. This dilemma led us to explore a simplified kinetic method with which regional MRglc can be estimated with a single static image acquired between 45 and 60 min after injection of 18F-FDG and with a correction for blood glucose concentration in the beginning and 18F-FDG activity at the end of the 18F-FDG PET imaging (26). It was noted from our earlier study that the coefficient of determination between MRglc measured with the dynamic method and estimated using the simplified method was 0.96, 0.94, and 0.98 for pretherapy, posttherapy, and pooled data, respectively. Thus, it indicates that the observed tumor uptake of 18F-FDG between 45 and 60 min after administration, corrected for blood 18F-FDG activity and glucose concentration, can reliably predict MRglc from a single static image acquired between 45 and 60 min.

Torizuka *et al.* (59) compared regional MRglc, measured with a dynamic method and a three-compartment model [$K_i = K_{1k3}/(k_2 + k_3)$] with SUV normalized for lean body weight (SUV_{lean}) obtained 50–60 min after 18F-FDG injection in patients with untreated primary lung cancer ($n = 19$). The estimate of the net 18F-FDG phosphorylation rate, $K_i = K_{1k3}/(k_2 + k_3)$, correlated highly with SUV_{lean} in lung cancer with a correlation coefficient of 0.937. However, the correlation between k_3 alone and SUV_{lean} was poor, with a correlation coefficient of 0.032. Thus, the combination of facilitated transportation of FDG (Glut-1) and k_3 seem to be the major contributors to the total accumulation of FDG in lung cancer. Therefore, the authors concluded that the kinetic data of FDG uptake are expected to be robust in assessing the biologic activity of lung cancer and monitoring therapy response. Minn *et al.* (60) evaluated the reproducibility of quantitative measurement of FDG uptake in 10 patients with untreated lung cancer by performing two dynamic FDG PET studies after a 4-h fast within 1 week. Kinetic modeling of tumor FDG uptake was performed on the basis of a three-compartment model. The mean difference was $6\% \pm 6\%$ (standard deviation) and $6\% \pm 5\%$ for SUV_{lean} and FDG influx constant K_i over the repeated PET scans.

The simplified kinetic method developed by us for measuring regional MRglc in lung cancer showed a good inverse correlation between residual MRglc and pTCP. Lucignani *et al.* (61) conducted 120-min dynamic FDG PET studies in 4 healthy and normal human subjects in searching for an optimal yet practical procedure for the determination of regional MRglc in heterogeneous tissues of brain. Regional MRglc was determined at various intervals up to 120 min after administration of 18F-FDG to determine the set of rate constants and best time for the determination of regional MRglc with the three-rate constant model and single-scan procedure. When the regional MRglc, measured by dynamic scanning at 0–30, 0–75, and 0–120 min after the injection of 18F-FDG, correlated with that of the single-scan method, the coefficient of determination was 0.994. It was concluded that regional MRglc could be measured with three-rate constant model, combined with the use of mass-

weighted average population rate constants and a single-scan procedure. Wakita *et al.* (62) also explored the possibility of replacing serial arterial sampling, which is required in dynamic quantitative 18F-FDG PET studies, with one point arterial or venous blood sampling in 120 patients with a variety of cerebral or suspected cerebral diseases, including brain tumor, cerebrovascular disease, epilepsy, and others. This study showed that the correlation between the estimated integral value determined by a one-point arterial blood sample at 12 min after the injection of 18F-FDG and the real integral value obtained by multiple arterial blood sampling was quite excellent with the coefficient of determination 0.9974 ($n = 120$). The correlation between the estimated integral value determined by a one-point venous blood sample at 40 min after injection, and the real integral value obtained by multiple arterial blood sampling was also excellent with a coefficient of determination of 0.9966 ($n = 10$). The percentage of error of the integral value estimated was 1.7% with arterial blood at 12 min ($n = 120$) compared with 3.64% with venous blood at 40 min ($n = 10$). The authors concluded that the simplified one-point sample method works in a manner that is comparable with serial arterial sampling and should be useful in clinical PET. Therefore, the results of the studies by Lucignani *et al.* (61) and Wakita *et al.* (62) are supportive of our study and results using the simplified kinetic method.

We used a preoperative radiation dose schedule of 42–54 Gy in 1.5-Gy fractions twice daily for the total dose of 42 Gy ($n = 15$) and 45–54 Gy in 1.8–2.0-Gy fractions, five fractions weekly ($n = 13$), which was judged unlikely to cause a significant decrease in blood supply (nutrient) to the tumor. Therefore, it is reasonable to assume that a possible decrease in nutrient supply to the tumor as a result of the preoperative therapy is unlikely to be a significant contributing factor to the dose–response relationship between residual FDG uptake and pTCP. Indeed, Thews *et al.* (63) showed that there was an increase in the tissue glucose level from $0.38 \pm 0.17 \mu\text{mol/g}$ at 0 Gy (control) to $1.20 \pm 0.23 \mu\text{mol/g}$ at 45 Gy in 15 fractions within 3 weeks and no decrease in the partial pressure of oxygen in an experiment in which a rat model of R1H rhabdomyosarcoma was treated with fractionated radiation of 75 Gy in 25 fractions within a 5-week period. Although the concentration of adenosine triphosphate and lactate steadily declined as the radiation dose was increased, the glucose concentration increased approximately linearly throughout the entire period of RT. Thus, they concluded that the increase in tissue glucose level, paralleled with the increment in total radiation dose, might be the result of a reduced glucose demand by the tumor because of a decrease in the number of tumor cells for a concurrent decrease in tumor volume was present.

Other factors that influence the magnitude of residual FDG uptake after RT or chemoradiotherapy include the timing of the study after RT completion and the proportion of FDG uptake contributed by inflammatory and tumor stromal cells. A hallmark of cellular response to radiation is the loss of the capacity for sustained proliferation (28–30).

The time course for tumor cells that lose viability (biologically dead but metabolically active) as a result of lethal radiation damage to undergo pyknosis or lysis depends on the proliferative activity of tumor cells. Tumor cells with a high mitotic index would be expected to regress rapidly after RT (i.e., small-cell lung cancer). The time course for NSCLC cells to undergo lysis after being inflicted with lethal radiation damage remains to be determined. However, clinical observation suggests that it may take 8–12 weeks for biologically lethally damaged cancer cells of NSCLC to undergo lysis. Therefore, the value of MRglc obtained 2 weeks after RT or chemoradiotherapy, such as was done in this study, is likely higher than the value attainable if FDG PET were done 2 months after RT. However, such a delay in obtaining FDG PET after therapy may not be helpful if the treatment course were supplemented with a boost dose of radiation according to the value of residual FDG uptake, because a long break in fractionated RT has a significantly negative impact in achieving tumor control.

Tumor stromal cells and infiltrated inflammatory cells may have made a contribution to the overall FDG uptake. According to the study by Brown *et al.* (64), monocytes/macrophages defined by CD68-positive staining in resected NSCLC without preoperative therapy ($n = 23$) accounted for $7.4\% \pm 6.4\%$ of all cells (range 0–22%). Infiltrating inflammatory white blood cells positive for Glut-3 (glucose transporter protein-3) also represented a small fraction of the tissue sample. Therefore, they concluded that the contribution by noncancerous elements to the overall FDG uptake was probably not substantial. Marom *et al.* (65) also correlated FDG uptake with Glut-1 and Glut-3 expression in early-stage lung cancer of 73 patients. Their study showed a linear relationship between SUV and tumor size, but not with Glut-1 or Glut-3.

Technical factors that affect the accurate measurement of MRglc include in-plane resolution of an imaging system that is 7 mm^3 , object size, object geometry, and size and shape of the ROI. Thus, an object size smaller than about 15 mm will result in significant underestimation of the true value of MRglc. The biologic heterogeneity of tumors that affect the accurate measurement of MRglc includes the fractions of proliferating tumor cells, amount of inflammatory/stromal cells in tumor, and degree of differentiation of NSCLC. Although regional MRglc measured with dynamic method is highly reproducible (60), absolute values of regional MRglc need to be considered with caution, because LC values, which indicate the different affinities of FDG

and glucose for transportation and phosphorylation, are not yet fully clarified for cancer cells (55).

Despite the shortcomings of the current FDG PET study in lung cancer, the correlation seen in this study between the residual MRglc reflecting the status of regional glucose use by residual lung cancer after preoperative chemoradiotherapy and the rate of histopathologic complete response is of clinical significance. The inverse correlation we observed between the residual amount of MRglc and pTCP supports the hypothesis that no uptake is strong evidence for no residual cells. The significance of the pretherapy value of MRglc in predicting the tumor response to chemoradiotherapy remains to be determined. This will be pursued in the future.

Residual MRglc with corresponding pTCP may be a surrogate biomarker for therapy response. Residual MRglc $\leq 0.040 \text{ } \mu\text{mol}/\text{min}/\text{g}$ corresponds to almost 99.9% pTCP and may represent a biochemically complete response. An incorporation of FDG uptake data with corresponding pTCP into the gross target volume (GTV) defined with CT image would result in a 3D biologic target volume for 3D conformal therapy. Indeed, an improvement in outlining the GTV for RT has also been reported by combining both CT and FDG PET images (66–68). With the advent of intensity-modulated RT technology, it is feasible that the radiation dose/dose intensity can be allocated according to the distribution/magnitude of the biologic target volume within the GTV to attain the highest possible tumor control. Radiation dose-painting in two-dimensional or dose-sculpting in 3D planning has been alluded to by Ling *et al.* (69) as a means of differential allocation of radiation dose/dose intensity according to the size and distribution of the biologic target volume within the GTV.

CONCLUSION

The data of regional MRglc measured with the dynamic method initially and later with the simplified kinetic method represents at best surrogate values. Nonetheless, this surrogate quantity showed a good correlation between residual regional MRglc after chemoradiotherapy and the degree of pathologic tumor control in locally advanced-stage NSCLC. The relationship between pTCP and the gradient of residual MRglc after RT or chemoradiotherapy is an inverse correlation. Residual MRglc corresponding to pTCP 50% and pTCP $\geq 95\%$ was $0.076 \text{ } \mu\text{mol}/\text{min}/\text{g}$ and $\leq 0.040 \text{ } \mu\text{mol}/\text{min}/\text{g}$, respectively. The gradient of residual MRglc with corresponding pTCP represents the residual biologic target volume within the tumor mass.

REFERENCES

1. Perez CA, Stanley K, Rubin P, *et al.* A prospective randomized study of various radiation doses and fractionation schedules in the treatment of inoperable non-oat-cell carcinoma of the lung: Preliminary report by the Radiation Therapy Oncology Group. *Cancer* 1980;45:2744–2753.
2. Choi NCH, Doucette JA. Improved survival of patients with unresectable non-small-cell bronchogenic carcinoma by an innovated high-dose en-bloc radiotherapeutic approach. *Cancer* 1981;48:101–109.
3. Dillman RO, Herndon J, Seagren SL, *et al.* Improved survival

- in stage III non-small cell lung cancer: Seven-year follow-up of Cancer and Leukemia Group B (CALGB) 8433 Trial. *J Natl Cancer Inst* 1996;88:1210–1215.
4. Sause WT, Scott C, Taylor S, *et al.* Radiation Therapy Oncology Group 88-08 and Eastern Cooperative Oncology Group 4588: Preliminary results of a phase III trial in regionally advanced, unresectable non-small-cell lung cancer. *J Natl Cancer Inst* 1995;87:198–205.
 5. Arriagada R, Le Chevalier T, Quoix E, *et al.*, for the GETCB, the FNCLCC, and the CEBI trialists. ASTRO plenary—Effect of chemotherapy on locally advanced non-small cell lung carcinoma: A randomized study of 353 patients. *Int J Radiat Oncol Biol Phys* 1991;20:1183–1190.
 6. Le Chevalier T, Arriagada R, Quoix E, *et al.* Radiotherapy alone versus combined chemotherapy and radiotherapy in nonresectable non-small cell lung cancer: First analysis of a randomized trial in 353 patients. *J Natl Cancer Inst* 1991;83:417–423.
 7. Arriagada R, Le Chevalier T, Rekecawicz C, *et al.*, for the CEBI-138 trialists, French Anticancer Centers. Cisplatin-based chemotherapy in patients with locally advanced non-small cell lung cancer: Late analysis of a French randomized trial [Abstract]. *Proc Am Soc Clin Oncol* 1997;16:446a.
 8. Saunders MI, Dische S, Barrett A, *et al.*, on behalf of the CHART Steering Committee. Continuous, hyperfractionated, accelerated radiotherapy (CHART) versus conventional radiotherapy in non-small-cell lung cancer: Mature data from the randomised multicenter trial. *Radiother Oncol* 1999;52:137–148.
 9. Cox JD, Azarnia N, Byhardt RW, *et al.* A randomized phase I/II trial of hyperfractionated radiation therapy with total doses of 60.0 Gy to 79.2 Gy—Possible survival benefit with greater than or equal to 69.6 Gy in favorable patients with Radiation Oncology Group stage III non-small cell lung carcinoma: Report of Radiation Therapy Oncology Group 83-11. *J Clin Oncol* 1990;8:1543–1555.
 10. Graham MV, Purdy JA, Enami B, *et al.* Preliminary results of a prospective trial using three dimensional radiotherapy for lung cancer. *Int J Radiat Oncol Biol Phys* 1999;33:993–1000.
 11. Rosenzweig KE, Mychalczak B, Fuks Z, *et al.* Final report of the 70.2-Gy and 75.6-Gy dose levels of a phase I dose escalation study using three-dimensional conformal radiotherapy in the treatment of inoperable non-small cell lung cancer. *Cancer J* 2000;6:82–87.
 12. Socinski MA, Rosenman J, Halle J, *et al.* Dose-escalating conformal radiation therapy with induction and concurrent carboplatin/paclitaxel in unresectable stage IIIA/B non-small cell lung carcinoma. *Cancer* 2001;92:1213–1223.
 13. Hayman JA, Martel MK, Ten Haken RK, *et al.* Dose escalation in non-small-cell lung cancer using three-dimensional conformal radiation therapy: Update of a phase I trial. *J Clin Oncol* 2001;19:127–136.
 14. Maguire PD, Marks LB, Sibley GS, *et al.* 73.6 Gy and beyond: Hyperfractionated, accelerated radiotherapy for non-small-cell lung cancer. *J Clin Oncol* 2001;19:705–711.
 15. Pujol JL, Demoly P, Daures JP, *et al.* Chest tumor response measurement during lung cancer chemotherapy: Comparison between computed tomography and standard roentgenography. *Am Rev Respir Dis* 1992;145:1149–1154.
 16. Parrat E, Pujol JL, Gautier V, *et al.* Chest tumor response during lung cancer chemotherapy: Computed tomography vs fiberoptic bronchoscopy. *Chest* 1993;103:1495–1501.
 17. Sugarbaker DJ, Herndon J, Kohman LJ, *et al.* Results of Cancer and Leukemia Group B Protocol 8935: A multi-institutional Phase II trimodality trial for stage III A (N2) non-small-cell lung cancer. *J Thorac Cardiovasc Surg* 1995;109:473–485.
 18. Rusch V, Giroux DJ, Kraut MJ, *et al.* Induction chemoradiation and surgical resection for non-small cell lung carcinomas of the superior sulcus: Initial results of Southwest Oncology Group Trial 9416 (Intergroup trial 0160). *J Thorac Cardiovasc Surg* 2001;121:472–483.
 19. Warburg O. On the origin of cancer cells. *Science* 1956;123:309–314.
 20. Isselbacher KJ. Increased uptake of amino acids and 2-deoxy-d-glucose by virus-transformed cells in culture. *Proc Nat Acad Sci USA* 1972;69:585–589.
 21. Flier JS, Mueckler MM, Usher P, *et al.* Elevated levels of glucose transport and transporter messenger RNA are induced by ras or src oncogenes. *Science* 1987;235:1494–1495.
 22. Sokoloff L, Reivich M, Kennedy C, *et al.* The [¹⁴C]deoxy-glucose method for the measurement of local cerebral glucose utilization: Theory, procedure, and normal values in the conscious and anesthetized albino rat. *J Neurochem* 1977;28:897–916.
 23. Phelps ME, Huang S-C, Hoffman EL, *et al.* Tomographic measurement of local cerebral glucose metabolic rate in humans with (F-18)-2-fluoro-2-deoxy-d-glucose: Validation of method. *Ann Neurol* 1979;6:371–388.
 24. Patlak CS, Blasberg RG, Fenstermacher JD. Graphical evaluation of blood-to-brain transfer constants from multiple-time uptake data. *J Cereb Blood Flow Metab* 1983;3:1–7.
 25. Hamberg L, Hunter G, Alpert N, *et al.* The dose uptake ratio: Useful parameter or over simplification? *J Nucl Med* 1994;35:1308–1312.
 26. Hunter GJ, Hamberg LM, Alpert N, *et al.* Simplified measurement of deoxyglucose utilization rate. *J Nucl Med* 1996;37:950–955.
 27. Fischman AJ. Editorial: Positron emission tomography in the clinical evaluation of metastatic cancer. *J Clin Oncol* 1996;14:691–696.
 28. Suit HD. Clinical radiation biology. In: Choi NC, Grillo HC, editors. Thoracic oncology. New York: Raven Press; 1983. p. 51–58.
 29. Thompson LH, Suit HD. Proliferation kinetics of x-irradiation mouse L cells studies with time-lapse photography. *Int J Radiat Biol* 1969;15:347–363.
 30. Sinclair WK. X-ray induced heritable damage (small colony formation) in cultured mammalian cells. *Radiat Res* 1964;21:584–611.
 31. Choi NC, Carey RW, Daly W, *et al.* Potential impact on survival of improved downstaging and resection rate by pre-operative twice-daily radiation and concurrent chemotherapy in stage IIIA non-small-cell lung cancer. *J Clin Oncol* 1997;15:712–722.
 32. Gambhir SS, Schwaiger M, Huang SC, *et al.* Simple noninvasive quantification method for measuring myocardial glucose utilization in humans employing positron emission tomography and fluorine-18 deoxyglucose. *J Nucl Med* 1989;30:359–366.
 33. Niemierko A, Goitein M. Implementation of a model for estimating tumor control probability for an inhomogeneously irradiated tumor. *Radiother Oncol* 1993;29:140–147.
 34. Niemierko A, Goitein M. Modeling of normal tissue response to radiation: The critical volume model. *Int J Radiat Oncol Biol Phys* 1993;25:135–145.
 35. Niemierko A, Goitein M. Dose-volume distributions: A new approach to dose-volume histograms in three-dimensional treatment planning. *Med Phys* 1994;21:3–11.
 36. Berbaum KS, Dorfman DD, Franken EA Jr. Measuring observer performance by ROC analysis: Indications and complications. *Invest Radiol* 1989;24:228–233.
 37. Metz CE. Some practical issues of experimental design and data analysis in radiological ROC studies. *Invest Radiol* 1989;24:234–245.
 38. Hoekstra CJ, Paglianiti I, Hoekstra OS, *et al.* Monitoring

- response to therapy in cancer using [18F]-2-fluoro-2-deoxy-d-glucose and positron emission tomography: An overview of different analytical methods. *Eur J Nucl Med* 2000;27:731–743.
39. Nolop KB, Rhodes CG, Brudin LH, *et al.* Glucose utilization in vivo by human pulmonary neoplasms. *Cancer* 1987;60:2682–2689.
 40. Patz EJ, Lowe VJ, Hoffman JM, *et al.* Focal pulmonary abnormalities: Evaluation with F-18 fluorodeoxyglucose PET scanning. *Radiology* 1993;188:487–490.
 41. Wahl RL, Quint LE, Greenough RL, *et al.* Staging of mediastinal non-small cell lung cancer with FDG PET, CT, and fusion images: Preliminary prospective evaluation. *Radiology* 1994;191:371–377.
 42. Dewan NA, Gupta NC, Redepenning LS, *et al.* Diagnostic efficacy of PET-FDG imaging in solitary pulmonary nodules: Potential role in evaluation and management. *Chest* 1993;104:997–1002.
 43. Dwamena BA, Sonnad SS, Angobaldo JO, *et al.* Metastases from non-small cell lung cancer: Mediastinal staging in the 1990s—Meta-analytic comparison of PET and CT. *Radiology* 1999;213:530–536.
 44. Pieterman RM, van Putten JW, Meuzelaar JJ, *et al.* Preoperative staging of non-small-cell lung cancer with positron emission tomography. *N Engl J Med* 2000;343:254–261.
 45. MacManus MP, Hicks RJ, Matthew JP, *et al.* High rate of detection of unsuspected distant metastases by PET in apparent stage III non-small-cell lung cancer: Implications for radical radiation therapy. *Int J Radiat Oncol Biol Phys* 2001;50:287–293.
 46. Gupta NC, Graeber G, Bishop HA. Comparative efficacy of positron emission tomography with fluorodeoxyglucose in evaluation of small (<1 cm), intermediate (1 to 3 cm), and large (>3 cm) lymph node lesions. *Chest* 2000;117:773–778.
 47. Kalff V, Rodney J, Hicks MP, *et al.* Clinical impact of 18F fluorodeoxyglucose positron emission tomography in patients with non-small-cell lung cancer: A prospective study. *J Clin Oncol* 2001;19:111–118.
 48. Inoue T, Kim EE, Komaki R, *et al.* Detecting recurrent or residual lung cancer with FDG-PET. *J Nucl Med* 1995;36:788–793.
 49. Hicks RJ, Kalff V, MacManus MP, *et al.* The utility of 18F-FDG PET for suspected recurrent non-small cell lung cancer after potentially curative therapy: Impact on management and prognostic stratification. *J Nucl Med* 2001;42:1605–1613.
 50. Zhuang H, Pourdehnad M, Lambright ES, *et al.* Dual time point 18F-FDG PET imaging for differentiating malignant from inflammatory processes. *J Nucl Med* 2001;42:1412–1417.
 51. Calvo R, Marti-Climent JM, Richter JA, *et al.* Three-dimensional clinical PET in lung cancer: Validation and practical strategies. *J Nucl Med* 2000;41:439–448.
 52. Hustinx R, Smith RJ, Benard F, *et al.* Dual time point fluorine-18 fluorodeoxyglucose positron emission tomography: A potential method to differentiate malignancy from inflammation and normal tissue in the head and neck. *Eur J Nucl Med* 1999;26:1345–1348.
 53. Boerner AR, Weckesser M, Herzog H, *et al.* Optimal scan time for fluorine-18 fluorodeoxyglucose positron emission tomography in breast cancer. *Eur J Nucl Med* 1999;26:226–230.
 54. Lowe VJ, DeLong DM, Hoffman JM, *et al.* Optimum scanning protocol for FDG-PET evaluation of pulmonary malignancy. *J Nucl Med* 1995;36:883–887.
 55. Keyes JW Jr. SUV: Standard uptake or silly useless value? *J Nucl Med* 1995;36:1836–1839.
 56. Gordon BA, Flanagan FL, Dehdashti F. Whole-body positron emission tomography: Normal variations, pitfalls, and technical considerations. *AJR Am J Roentgenol* 1997;169:1675–1680.
 57. Shreve PD, Anzai Y, Wahl RL. Pitfalls in oncologic diagnosis with FDG PET imaging: Physiologic and benign variants. *Radiographics* 1999;19:61–77.
 58. Higashi K, Ueda Y, Seki H, *et al.* Fluorine-18-FDG imaging is negative in bronchioloalveolar lung carcinoma. *J Nucl Med* 1998;39:1016–1020.
 59. Torizuka T, Zasadny KR, Recker B, *et al.* Untreated primary lung and breast cancers: Correlation between F-18 FDG kinetic rate constants and findings of in vitro studies. *Radiology* 1998;207:767–774.
 60. Minn H, Zasadny KR, Quint LE, *et al.* Lung cancer: Reproducibility of quantitative measurements for evaluating 2-[F-18]-fluoro-2-deoxy-d-glucose uptake at PET. *Radiology* 1995;196:167–173.
 61. Lucignani G, Schmidt KC, Moresco RM, *et al.* Measurement of regional cerebral glucose utilization with fluorine-18-FDG and PET in heterogeneous tissues: Theoretical considerations and practical procedure. *J Nucl Med* 1993;34:360–369.
 62. Wakita K, Imahori Y, Ido T, *et al.* Simplification for measuring input function of FDG PET: Investigation of 1-point blood sampling method. *J Nucl Med* 2000;41:1484–1490.
 63. Thews O, Zywiets F, Lecher B, *et al.* Quantitative changes of metabolic and bioenergetic parameters in experimental tumors during fractionated irradiation. *Int J Radiat Oncol Biol Phys* 1999;45:1281–1288.
 64. Brown RS, Leung JY, Kison PV, *et al.* Glucose transporters and FDG uptake in untreated primary human non-small cell lung cancer. *J Nucl Med* 1999;40:556–565.
 65. Marom EM, Aloia TA, Moore MB, *et al.* Correlation of FDG-PET imaging with Glut-1 and Glut-3 expression in early-stage non-small cell lung cancer. *Lung Cancer* 2001;33:99–107.
 66. Nestle U, Walter K, Schmidt S, *et al.* 18F-deoxyglucose positron emission tomography (FDG-PET) for the planning of radiotherapy in lung cancer: High impact in patients with atelectasis. *Int J Radiat Oncol Biol Phys* 1999;44:593–597.
 67. Kiffer JD, Berlangieri SU, Scott AM, *et al.* The contribution of 18F-fluoro-2-deoxy-glucose positron emission tomographic imaging to radiotherapy planning in lung cancer. *Lung Cancer* 1998;19:167–177.
 68. Caldwell CB, Mah K, Ung YC, *et al.* Observer variation in contouring gross tumor volume in patients with poorly defined non-small-cell lung tumors on CT: The impact of 18FDG-hybrid PET fusion. *Int J Radiat Oncol Biol Phys* 2001;51:923–931.
 69. Ling CC, Humm J, Larson S, Amols H, *et al.* Towards multidimensional radiotherapy (MD-CRT). *Int J Radiat Oncol Biol Phys* 2000;47:551–560.